PCCP

Cite this: *Phys. Chem. Chem. Phys.*, 2011, **13**, 8515–8525

www.rsc.org/pccp

PAPER

Exploring the dynamics of reaction $N(^2D) + C_2H_4$ with crossed molecular-beam experiments and quantum-chemical calculations

Shih-Huang Lee,*[ab] Chih-Hao Chin,[a] Wei-Kan Chen,[a] Wen-Jian Huang[a] and Chu-Chun Hsieh[ab]

Received 7th November 2010, Accepted 4th March 2011
DOI: 10.1039/c0cp02439b

We conducted the title reaction using a crossed molecular-beam apparatus, quantum-chemical calculations, and RRKM calculations. Synchrotron radiation from an undulator served to ionize selectively reaction products by advantage of negligibly small dissociative ionization. We observed two products with gross formula C_2H_3N and C_2H_2N associated with loss of one and two hydrogen atoms, respectively. Measurements of kinetic-energy distributions, angular distributions, low-resolution photoionization spectra, and branching ratios of the two products were carried out. Furthermore, we evaluated total branching ratios of various exit channels using RRKM calculations based on the potential-energy surface of reaction $N(^2D) + C_2H_4$ established with the method CCSD(T)/6-311+G(3df,2p)//B3LYP/6-311G(d,p)+ZPE[B3LYP/6-311G(d,p)]. The combination of experimental and computational results allows us to reveal the reaction dynamics. The $N(^2D)$ atom adds to the C=C π-bond of ethene (C_2H_4) to form a cyclic complex *c*-$CH_2(N)CH_2$ that directly ejects a hydrogen atom or rearranges to other intermediates followed by elimination of a hydrogen atom to produce C_2H_3N; *c*-$CH_2(N)CH + H$ is the dominant product channel. Subsequently, most C_2H_3N radicals, notably *c*-$CH_2(N)CH$, further decompose to $CH_2CN + H$. This work provides results and explanations different from the previous work of Balucani *et al.* [*J. Phys. Chem. A*, 2000, **104**, 5655], indicating that selective photoionization with synchrotron radiation as an ionization source is a good choice in chemical dynamics research.

I. Introduction

Dinitrogen (N_2) is the most abundant molecule in the atmosphere but too inert to react with other atmospheric molecules due to the strong N≡N triple bond. In contrast, atomic nitrogen, particularly in an electronic excited state, could react with some atmospheric molecules. The chemistry of nitrogen atoms plays an important role in the atmosphere because nitrogen atoms can be produced from nitrogen-containing molecules, notably N_2, by cosmic radiation and lightning. In laboratories nitrogen atoms are producible typically from N_2 by various discharge approaches.

Atomic nitrogen with an electronic configuration of $1s^22s^22p^3$ has three lowest-lying electronic states ^4S, ^2D and ^2P. State ^2D lies 2.38 eV and ^2P 3.576 eV above the ground state ^4S.[1] Nitrogen atoms in state ^2D are believed to be more reactive than in states ^4S and ^2P based on measurements of rate coefficients of reactions of nitrogen atoms with various molecules.[2] A nitrogen atom in state ^2D has a radiative lifetime of 17 h,[1] which makes feasible the reaction of atomic $N(^2D)$ with other molecules in experiments. Thus, most studies on reaction dynamics of nitrogen atoms were devoted to the reactions of ^2D nitrogen atoms with H_2/D_2,[3–5] H_2O,[6] CH_4,[7–9] SiH_4,[10,11] C_2H_2,[12,13] and C_2H_4.[14–16] Reactions started with an insertion mechanism of $N(^2D)$ atoms into bonds H–H, CH_3–H and SiH_3–H to form reaction complexes H–N–H, CH_3–N–H and SiH_3–N–H, as well as an addition mechanism to the π-bond of CH≡CH and CH_2=CH_2 to form cyclic complexes *c*-CH(N)CH and *c*-$CH_2(N)CH_2$, respectively. The complexes underwent either direct decomposition or various isomerization processes followed by decomposition. Two product channels $SiNH_2 + 2H$ and $SiNH + H_2 + H$ were reported for the $N(^2D) + SiH_4$ reaction whereas only single channels with the elimination of a hydrogen atom were reported for the reactions of $N(^2D)$ with H_2, CH_4, C_2H_2 and C_2H_4.

As for the title reaction $N(^2D) + C_2H_4$, a part of the doublet potential-energy surface (PES) was established by Takayanagi *et al.* using the method PMP4(SDTQ)/cc-pVTZ//MP2/cc-pVDZ.[14] The calculations predicted that the main reaction mechanism is addition of atomic $N(^2D)$ onto the C=C π-bond of C_2H_4 to form a three-membered cyclic complex *c*-$CH_2(N)CH_2$ that undergoes various pathways for elimination

[a] *National Synchrotron Radiation Research Center (NSRRC), 101 Hsin-Ann Road, Hsinchu Science Park, Hsinchu 30076, Taiwan*
[b] *Department of Applied Chemistry, National Chiao-Tung University, 1001 University Road, Hsinchu 30010, Taiwan. E-mail: shlee@nsrrc.org.tw; Fax: +886-3-578-3813; Tel: +886-3-578-0281*

of hydrogen atoms to form various C_2H_3N isomers. The authors calculated product branching ratios of c-$CH_2(N)CH_2$ with internal energy 104.3 kcal mol^{-1}, *i.e.*, zero collision energy (E_c) for reactant $N(^2D) + C_2H_4$, using Rice–Ramsperger–Kassel–Marcus (RRKM) theory based on the established *ab initio* PES.[14] The calculations predicted that c-$CH_2(N)CH + H$ is the dominant channel with a branching ratio of 0.848. Thermal rate coefficients of reaction $N(^2D) + C_2H_4$ in the temperature range 225–292 K were measured and expressible as $2.3 \times 10^{-10}\ e^{-E_a/kT}$ cm^3 molecule^{-1} s^{-1}; activation energy E_a equals 1.0 ± 0.1 kcal mol^{-1}, indicating a small barrier in the entrance channel.[15]

Balucani *et al.* conducted the title reaction at $E_c = 8$ kcal mol^{-1} in a crossed molecular-beam apparatus equipped with an electron-impact ionizer.[16] Product ions were observed at mass-to-charge ratios (m/z) 38–41 u. Because the signals at those m/z values have similar TOF spectra and laboratory angular distributions, the ions with $m/z = 41$ u were assigned to products with gross formula C_2H_3N and those ions with $m/z = 38$–40 u to daughter ions of C_2H_3N due to severe dissociative ionization. The authors employed the data recorded at $m/z = 40$ u for analysis because of large ion signals. The authors, however, might have ignored the possibility that the ions with $m/z = 41$ u are the isotopic variants of product C_2H_2N with loss of two hydrogen atoms, since the signal of $m/z = 40$ u is much larger than that of $m/z = 41$ u. If so, the signal of C_2H_2N isotopmers might overlap with the signal of product C_2H_3N at $m/z = 41$ u. Selective photoionization[17] can give a solution to this ambiguity.

The merits of photoionization with synchrotron vacuum-ultraviolet (VUV) radiation as an ionization source in studies of unimolecular photodissociation[17–19] and atom–molecule chemical reactions[11,20,21] have been described elsewhere. The advantage of negligibly small dissociative photoionization enabled the direct detection of reaction products C_2H_3N and C_2H_2N which were indistinguishable using electron-impact ionization. The present work corrected the previous experimental results[16] conducted with electron-impact ionization and explored more deeply the dynamics of the reaction of $N(^2D)$ with ethene (C_2H_4). To support the experimental observations, a comprehensive PES was established and RRKM calculations were also performed in the present work.

II. Experiments

The experimental apparatus and procedure have been described elsewhere;[11,20,21] thus, only a brief description is given here. The crossed molecular-beam apparatus comprised two source chambers, a reaction chamber and a detection chamber. One source chamber equipped with an Even–Lavie valve and a discharge device[22] served to generate a pulsed beam of nitrogen atoms. A mixture of 3% N_2 and 97% He was supersonically expanded from the Even–Lavie valve with a backing pressure of 104 psi. A discharge was synchronously ignited while a molecular nitrogen pulse passed through the discharge device driven with a high-voltage pulse of -1 kV and 10 μs. The N-atom beam was collimated with two successive skimmers. In the other source chamber, an Even–Lavie valve heated up to 110 °C served to expand supersonically neat ethene at a stagnation pressure of 54 psi. The pulsed molecular ethene beam was collimated with a skimmer. An L-shaped copper panel installed near the reaction region was chilled to 14 K to diminish the background pressure in the reaction region. The cold panel had a hole of diameter 3 mm in each side for penetration of both atomic and molecular beams that intercepted at 90° to each other in the reaction chamber. Nitrogen atoms and ethene had mean velocities of 1750 and 890 m s^{-1}, respectively, giving a collision energy of 4.3 kcal mol^{-1}. Reaction products were scattered into a whole solid angle but only the products flying towards an ion detector were ionized with undulator radiation after a free flight along a path of length 100.5 mm. The undulator radiation had photons with harmonic frequencies in addition to the desired photons with the fundamental frequency. A windowless gas cell installed on the beam line was filled with noble gas to absorb high harmonic photons. An additional optical filter of MgF_2 served to effectively suppress high harmonic photons when the energy of fundamental-frequency photons was less than 10 eV. The filtered VUV beam was focused into a size of diameter $\sim$1 mm in the ionization region. The flux was $\sim 1 \times 10^{16}$ photons s^{-1} and the energy resolution ($\Delta E/E$) was $\sim$4%. The photon energy was tunable on adjusting the gap of the undulator for the purpose of selective ionization. Ion optics extracted product cations into a quadrupole mass filter for selection of species with a specific m/z ratio. An ion detector of Daly type counted the selected cations and a multi-channel scaler (MCS) sampled ions into 4000 bins of 1 μs. Two trigger-pulse generators operating at 200 Hz synchronized the experimental components. A time-of-flight (TOF) spectrum of a product can be obtained after subtracting the ion flight interval from the total flight duration and a background from the raw signal if necessary. To obtain product TOF spectra at various laboratory scattering angles (Θ) between the N-atom beam and the detection axis, the source-chamber assembly was rotated from $\Theta = -20°$ to 110°.

III. Computations

The computational details have been described elsewhere;[11,20,23] thus, only a brief description is given here. We established a comprehensive potential-energy surface for the $N(^2D) + C_2H_4$ reaction using the method CCSD(T)/6-311+G(3df,2p)//B3LYP/6-311G(d,p) + ZPE[B3LYP/6-311G(d,p)]. Computations were conducted using a suite of programs Gaussian-03 in a computer equipped with four CPUs and 16 GB of memory. Structures of molecules at stationary and transition states (TS) were optimized at the level of B3LYP/6-311G(d,p); harmonic vibrational frequencies and zero-point energies (ZPE) of molecules at optimized structures were computed also at the same level of theory. In addition to the examination of the number of imaginary vibrational frequency, the calculation of intrinsic reaction coordinate (IRC) served to verify the connection of a transition structure with its reactant and product. Total energies of atomic and molecular species were computed at the level of CCSD(T)/6-311+G(3df,2p). The same computational method was applied also to molecular cations for the calculations of adiabatic ionization energy (IE). We calculated rate coefficients of individual reaction steps

for the multi-channel dissociation of reaction complex c-$CH_2(N)CH_2$ with E_c = 5 kcal mol^{-1} using RRKM theory[24–26] and variational transition state theory (VTST).[26,27] RRKM theory was applicable to a reaction path with a transition state whereas VTST theory to a barrierless reaction path. The microcanonical rate coefficient $k(E)$ of a reaction step can be expressed as $k(E) = \frac{\sigma}{h}\frac{W^{\neq}(E-E^{\neq})}{\rho(E)}$ using RRKM theory; σ is a symmetry factor (or reaction path degeneracy), h is the Plank constant, $W^{\neq}(E - E^{\neq})$ represents the number of states accessible in a transition structure with a barrier height $E^{\neq}$, and $\rho(E)$ denotes the density of states of a reactant with internal energy E in a reaction step. The values of $W^{\neq}(E - E^{\neq})$ and $\rho(E)$ were estimated using a direct-count method based on the computed harmonic vibrational frequencies. In the VTST calculations, we calculated $k(E)$ as a function of reaction coordinate $q^{\neq}$ assuming each molecular structure optimized along $q^{\neq}$ is a pseudo transition state. A minimal rate coefficient could be found along $q^{\neq}$ according to the equation $\frac{dk(E,q^{\neq})}{dq^{\neq}} = 0$. Kinetic master equations $\frac{d[C]_i}{dt} = \sum k_n[C]_j - \sum k_m[C]_i$ were constructed and solved using stationary-state approximation, where $[C]_i$ and $[C]_j$ are concentrations of species i and j at time t as well as k_n and k_m are microcanonical rate coefficients computed with the RRKM or VTST approach. At $t \rightarrow \infty$, product branching ratios can be yielded.

IV. Results and analysis

Different from the work of Balucani *et al.*,[16] we observed two reaction products with gross formula C_2H_3N at m/z = 41 u and C_2H_2N at 40 u. To verify our assignments, Fig. 1 presents the TOF spectra of both species with m/z = 41 and 40 u recorded at Θ = 44° with photoionization energies at 10.8, 11.7 and 15.1 eV. The species of m/z = 41 u has two features peaking around 90 and 160 μs but the species of m/z = 40 u has a single feature peaking around 100 μs in TOF distributions. The distinct TOF distributions indicate the presence of two reaction products; the two features of m/z = 41 u are ascribed to product C_2H_3N and the single feature of m/z = 40 u to product C_2H_2N. The species with m/z = 40 u (C_2H_2N) has a TOF distribution insensitive to photoionization energy in the range of 10.8–15.1 eV, indicating that the dissociative ionization from product C_2H_3N to $C_2H_2N^+$ is negligible compared with the ion signal of product C_2H_2N in this energy range. In contrast, the TOF distribution of species with m/z = 41 u varies with photoionization energy; the TOF distribution has two apparent features with photon energies at 10.8 and 11.7 eV but becomes similar to that of m/z = 40 u at 15.1 eV. The variation of TOF distributions is attributed to the contribution of isotopic variants of product C_2H_2N to the signal of m/z = 41 u. Based on the natural abundances 1.1 × 10^{-2} of ^{13}C, 3.66 × 10^{-3} of ^{15}N and 1.5 × 10^{-4} of ^{2}H atoms,[28] the isotopic ratio of 41 u to 40 u of C_2H_2N is expected to be about 0.026 because C_2H_2N has two carbon, two hydrogen and one nitrogen atoms. Fig. 1 shows that the peak signals of m/z = 40 u (C_2H_2N) recorded with photoionization energies 10.8, 11.7 and 15.1 eV are about 5, 7.4 and 20 counts per 10^3 pulses, respectively. Therefore, isotopic variants of C_2H_2N will have about 0.13, 0.19 and 0.52 counts per 10^3 pulses contributing to the peak signals of m/z = 41 u recorded with photons at 10.8, 11.7 and 15.1 eV, respectively. Because product C_2H_2N has a yield much greater and an ionization threshold higher than that of product C_2H_3N (*vide infra*), the isotopic contribution of C_2H_2N to m/z = 41 u becomes more significant when photoionization energy is much larger than the ionization threshold ~10 eV of C_2H_2N.[29] The TOF distributions of both species of m/z = 40 and 41 u become similar in appearance with photoionization energy larger than 15 eV, which accounts for the observation of Balucani *et al.* using electron-impact ionization.

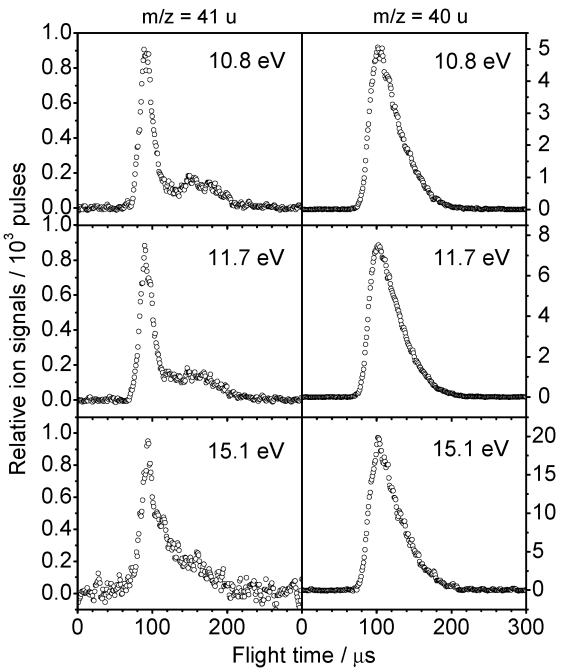

Fig. 1 TOF spectra of products with m/z = 41 u and 40 u recorded at Θ = 44° with photoionization energy 10.8, 11.7, and 15.1 eV. Left (right) ordinates show the relative ion signals of products with m/z = 41 (40) u normalized to 10^3 pulses. Each panel shows the photoionization energy employed.

Fig. 2 exhibits Newton diagrams associated with two-dimensional product velocity contours for the reactions of $N(^2D) + C_2H_4$ to $C_2H_3N + H$ and to $C_2H_2N + 2H$. In the laboratory frame, the flight direction of nitrogen atoms is defined as Θ = 0° and of ethene as Θ = 90°. $\Theta_{cm} \cong 46°$ is the flight direction of the center of masses (c.m.) of the reaction system. In the c.m. frame, the incident direction of nitrogen atoms is defined as θ = 0° and the opposite direction, *i.e.*, the incident direction of ethene, as θ = 180°. The scattering directions of reaction products C_2H_3N and C_2H_2N are called forward, sideways and backward for θ scanning from 0° through 90° to 180°. A simulation program served to mimic TOF spectra of products using forward convolution of initial guess c.m. kinetic-energy and angular distributions with experimental parameters. The transformation of signals from the laboratory frame to the c.m. frame was detailed in ref. 11. From the best fit to the experimental TOF spectra detected at various laboratory angles, angle-specific kinetic-energy distributions $P(E_t; \theta)$ and an angular distribution $P(\theta)$ of products in the c.m. frame are derivable. E_t denotes the total kinetic energy of two

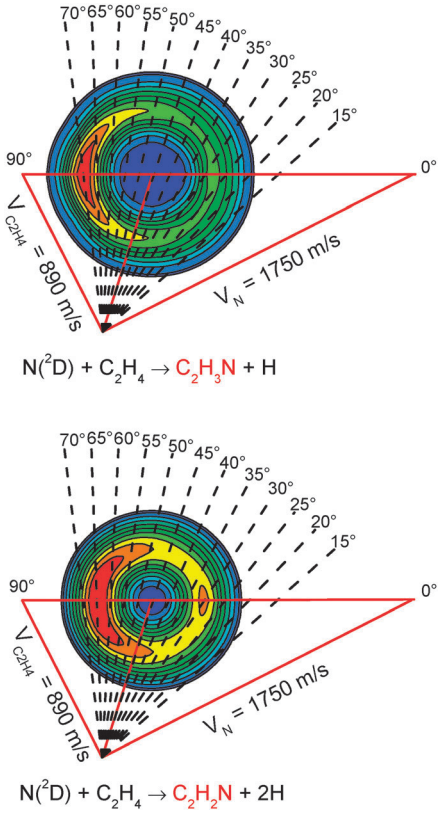

Fig. 2 Newton diagrams and two-dimensional product velocity contours for the reactions of $N(^2D) + C_2H_4 \rightarrow C_2H_3N + H$ and $N(^2D) + C_2H_4 \rightarrow C_2H_2N + 2H$. Dashed lines denote the detection axes at laboratory angles 15°–70°.

momentum-matched products. The kinetic-energy distribution at any θ value is derivable by interpolation.

Fig. 3 presents the TOF spectra of species with m/z = 41 u from Θ = 15° to 70° using photoionization energies 9.6 eV and 11.7 eV which are below and above, respectively, the ionization threshold ~10 eV of product C_2H_2N.[29] The data with Θ larger than 70° incur interference of impurities in the ethene beam and thus are omitted here. With photoionization energy 9.6 eV, the feature along with red-line simulation is assigned to product C_2H_3N with loss of a hydrogen atom. Since C_2H_3N has a small velocity in the c.m. frame, the C_2H_3N products recoiled forward and backward with respect to the c.m. flying direction are observable in the laboratory frame and thus the TOF distributions of C_2H_3N near Θ_{cm} are bimodal. The isotopic variants of product C_2H_2N (blue line) that has an ionization threshold around 10 eV appear in the case of 11.7 eV. The blue components were simulated with the same kinetic-energy and angular distributions derived from the TOF spectra of product C_2H_2N (*vide infra*). The c.m. ratio of the red to the blue component was determined to be 0.89 : 0.11 from the best global fit to the experimental TOF spectra recorded at 11.7 eV. Fig. 4 exhibits $P(E_t)$ distributions at seven θ angles and the $P(\theta)$ distribution derived from the best simulation as shown in Fig. 3. Fig. 5 presents the low-resolution photoionization spectrum of species recorded at m/z = 41 u; ion signals were detected at Θ = 44° and integrated from 50 μs to 250 μs in the flight time. The photoionization spectrum was divided into two curves; the blue line denotes the photoionization spectrum of isotopic variants of product C_2H_2N (*vide infra*) and the red line denotes the photoionization spectrum of product C_2H_3N. The ratio of the red to blue curve is 0.77 : 0.23 at 11.7 eV determined from the partitioning of TOF spectra of m/z = 41 u recorded with photoionization energy 11.7 eV. Arrows indicate the adiabatic ionization energies of isomers CH_2NCH and *c*-$CH_2(N)CH$.

Fig. 6 presents the TOF spectra of species with m/z = 40 u from Θ = 15° to 70° using photoionization energy 11.7 eV. The feature along with simulation is assigned to product C_2H_2N with loss of two hydrogen atoms. Because hydrogen atoms are too elusive to be detected in the present work, we assume a two-body dissociation process with a product mass ratio of 40 : 2 to simulate the TOF spectra of product C_2H_2N. Fig. 7 exhibits $P(E_t)$ distributions at seven θ angles and the $P(\theta)$ distribution derived from the best simulation as shown in Fig. 6; the $P(E_t)$ and $P(\theta)$ distributions were employed also to simulate the blue components of m/z = 40 u shown in Fig. 3. Fig. 8 presents the low-resolution photoionization spectrum of product C_2H_2N; ion signals were detected at Θ = 44° and integrated from 60 μs to 240 μs in the flight time. Arrows indicate the adiabatic ionization energies of isomers CH_2NC and CH_2CN. The combination of product TOF spectra (Fig. 1, 3 and 6) and product photoionization spectra (Fig. 5 and 8) clearly indicates that there are two distinct products with gross formula C_2H_3N and C_2H_2N observed in the present work. Fig. 9 presents the doublet PES established for the $N(^2D) + C_2H_4$ reaction including various exit channels. The green and red paths are not calculated in the work of Takayanagi *et al.* Thick solid lines denote some likely pathways leading to products $C_2H_3N + H$ and $C_2H_2N + 2H$. CH_3NCH, CH_2CHNH and CH_3CNH have symmetry C_s and thus have *cis*- and *trans*-conformers according to the geometry of skeletons CNCH, CCNH, and CCNH, respectively, as shown in Fig. 9.

We obtained average kinetic-energy release $\langle E_t \rangle$ and fraction f_t of available energy (E_{ava}) in translation based on $\langle E_t \rangle = \int\int E_t\, P(E_t;\, \theta)\, dE_t\, d(\cos\theta) / \int\int P(E_t;\theta) dE_t\, d(\cos\theta)$ and $f_t = \langle E_t \rangle / E_{ava}$. Table 1 lists the values of E_{ava}, $\langle E_t \rangle$, and f_t for product channels $C_2H_3N + H$ and $C_2H_2N + 2H$. The E_{ava} values of the most-probable isomeric channels *c*-$CH_2(N)CH + H$ and $CH_2CN + 2H$ were adopted for the calculations of $\langle E_t \rangle$ and f_t. Table 2 summarizes the adiabatic ionization energies of six isomers of C_2H_3N and three isomers of C_2H_2N. The difference between calculated and experimental IE values is within ±0.3 eV for CH_3CN, CH_3NC, *c*-$CH_2(N)CH$ and CH_2CN; thus, the other calculated IE values might be reliable. Table 3 summarizes total branching ratios of various two-body dissociation channels predicted by RRKM and VTST calculations with E_c = 5 kcal mol^{-1}; branching of secondary dissociation is beyond the present calculations.

V. Discussion

Ignoring the initial angular momenta of reactants supersonically cooled, the total angular momentum $\vec{J}$ of a reaction system equals approximately the orbital angular momentum $\vec{L}$ of a two-particle collision system, *i.e.*, $\vec{J} \cong \vec{L} = \mu\vec{b} \times \vec{v}_{rel}$.[30] μ is a

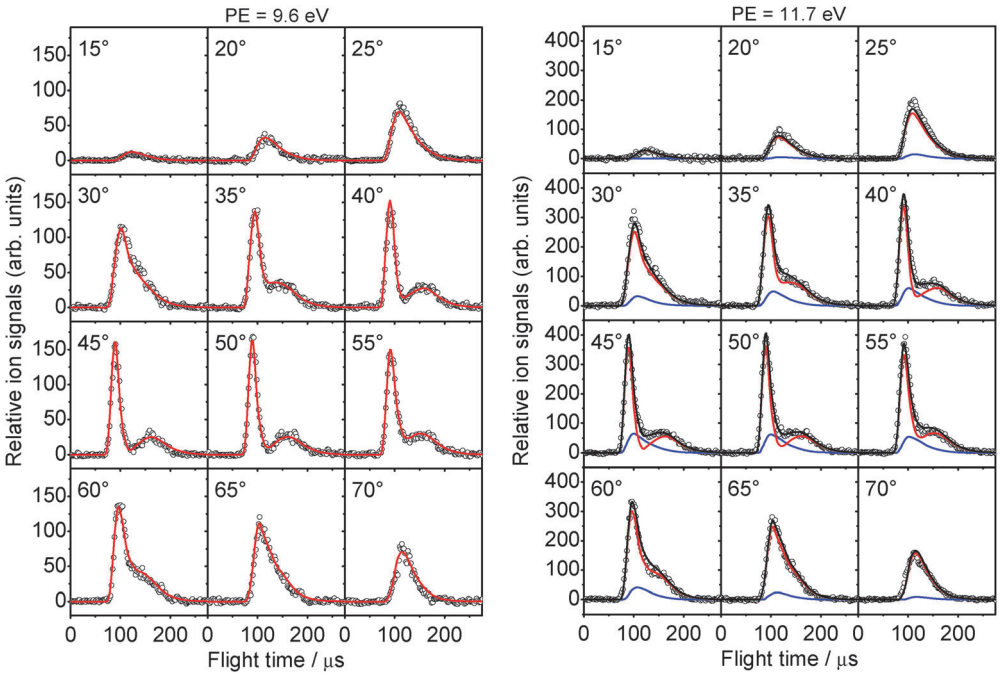

Fig. 3 Angle-specific TOF spectra of product C_2H_3N recorded at m/z = 41 u with photoionization energies 9.6 eV and 11.7 eV which are below and above, respectively, the ionization threshold ~10 eV of product C_2H_2N. Open circles denote the experimental data and solid curves denote the simulations. Each panel shows the corresponding laboratory angle Θ. Only C_2H_3N (red curve) is observable with photon energy at 9.6 eV whereas the isotopic variant of C_2H_2N (blue curve) additionally appears with photon energy at 11.7 eV. Black curves in the case of 11.7 eV are the sums of red and blue curves. Fig. 4 and 7 present the corresponding kinetic-energy and angular distributions for the red and blue components, separately.

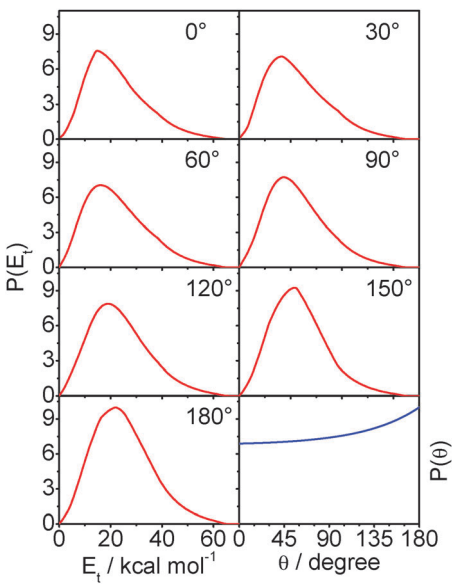

Fig. 4 Angle-specific distributions of kinetic energy and the angular distribution of product C_2H_3N.

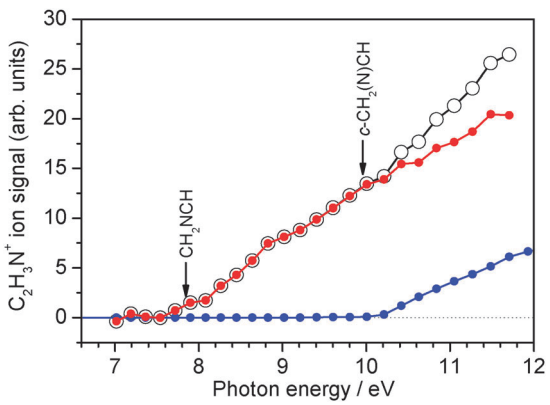

Fig. 5 Low-resolution photoionization spectrum of product C_2H_3N recorded at m/z = 41 u. Ion signals were detected at Θ = 44° and integrated from 50 μs to 250 μs in the flight time. The step increment is *ca.* 0.2 eV. Black open circles denote the experimental data. Blue circles represent the photoionization spectrum of product C_2H_2N same as that shown in Fig. 8 with a weighting according to the isotopic natural abundance. Red circles, the differences between the black and blue circles, represent the photoionization spectrum of product C_2H_3N. The ratio of the red to blue circle at 11.7 eV is 0.77 : 0.23 in the laboratory frame. Arrows indicate the calculated adiabatic ionization energies of CH_2NCH and *c*-$CH_2(N)CH$.

reduced mass, $\vec{b}$ is an impact parameter, and $\vec{v}_{rel}$ is the relative velocity between two colliding reactants. Parameter $\vec{b}$ is perpendicular to and randomly polarized about axis $\vec{v}_{rel}$. The opacity function $P(b)$, a reaction probability as a function of b, governs the dynamics of a two-particle collision.[30] The spatial distribution of reaction products has a symmetric axis along vector $\vec{v}_{rel}$ in the c.m. frame. For a direct reaction with a transient complex, the product angular distribution is dynamically controlled and typically forward–backward asymmetric.[30] In contrast, for a reaction with a persisting (long-lived) complex the original memory in dynamics becomes obscure and the angular distribution approaches forward-backward symmetric due to rotation of the reaction complex before decomposition.[30,31]

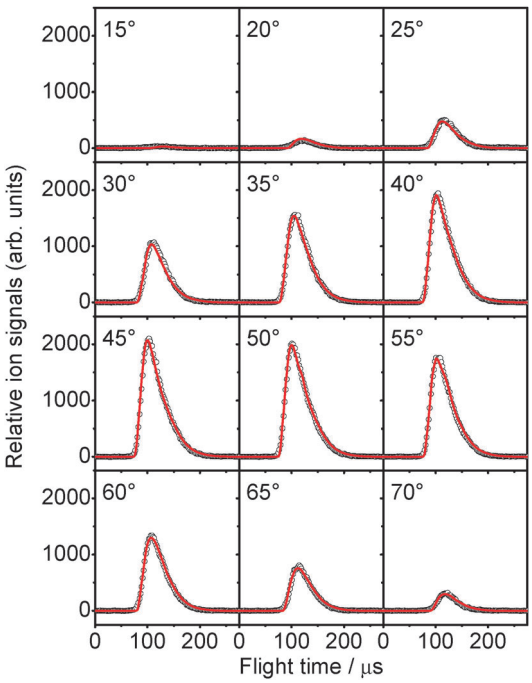

Fig. 6 Angle-specific TOF spectra of product C_2H_2N recorded at m/z = 40 u with photoionization energy 11.7 eV. Open circles denote the experimental data and solid curves denote the simulations. Each panel shows the corresponding laboratory angle Θ.

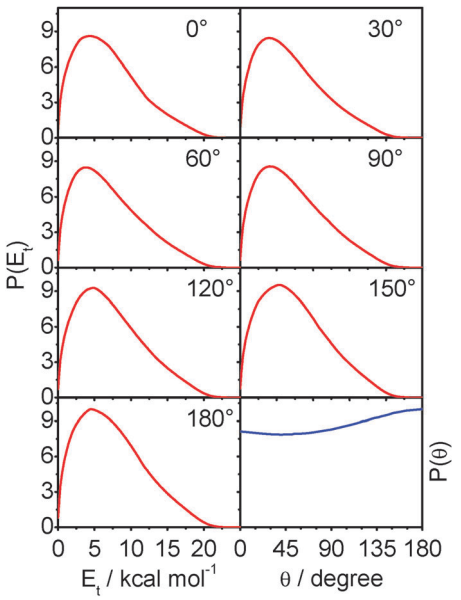

Fig. 7 Angle-specific distributions of kinetic energy and the angular distribution of product C_2H_2N.

Since the reactivity of nitrogen atoms in states ^4S and ^2P are typically much smaller than in state ^2D and the population of nitrogen atoms in state ^2P is less than in state ^2D,[11] reactions of $N(^4S)$ and $N(^2P)$ atoms with ethene are neglected here. Although the rate coefficient of $N(^2P)$ was close to $N(^2D)$ reactions with C_2H_4, the deactivation process of $N(^2P)$ was determined to be the spin-allowed quenching process $N(^2P) + C_2H_4(S_0) \rightarrow N(^4S) + C_2H_4(T_1)$.[15] The $N(^2D) + C_2H_4$

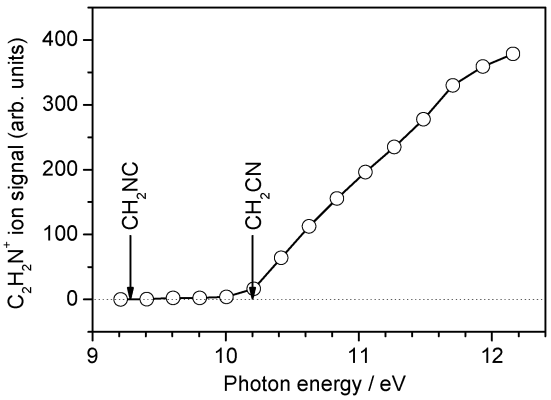

Fig. 8 Low-resolution photoionization spectrum of product C_2H_2N recorded at m/z = 40 u. Ion signals were detected at Θ = 44° and integrated from 60 μs to 240 μs in the flight time. The step increment is *ca.* 0.2 eV. Arrows indicate the calculated adiabatic ionization energies of CH_2NC and CH_2CN.

reaction starts with the addition of atomic $N(^2D)$ to the C=C π-bond of ethene to form *c*-$CH_2(N)CH_2$ through a small barrier at the entrance channel. Sato *et al.* reported an activation energy $E_a = 1.0 \pm 0.1$ kcal mol^{-1} for this reaction.[15] Takayanagi *et al.* reported a classical barrier height 3.2 kcal mol^{-1} for this addition process using a computational method CASSCF/cc-pVDZ; the barrier height was reduced to 1.6 kcal mol^{-1} with a correction of CASMP2 calculations but the location of the potential maximum shifted toward the reactant side.[14] The reaction complex *c*-$CH_2(N)CH_2$ subsequently undergoes either direct dissociation or a series of isomerization processes followed by decomposition mainly to $C_2H_3N + H$ and $C_2H_2N + 2H$ at exit channels (*vide infra*). The mechanism of atomic $N(^2D)$ inserting into bond C–H of ethene is negligible because of a significant entrance barrier that is 13 kcal mol^{-1} at the CASSCF(5,5)/cc-pVDZ level of theory.[14]

A Reaction $N(^2D) + C_2H_4 \rightarrow C_2H_3N + H$

Based on the PES shown in Fig. 9, the following lists some likely product channels for elimination of a hydrogen atom.

$$N(^2D) + C_2H_4 \rightarrow CH_3CN + H \qquad \Delta H^\circ = -107.6 \text{ kcal mol}^{-1} \quad (1)$$

$$\rightarrow CH_3NC + H \qquad \Delta H^\circ = -84.2 \text{ kcal mol}^{-1} \quad (2)$$

$$\rightarrow CH_2CNH + H \qquad \Delta H^\circ = -79.8 \text{ kcal mol}^{-1} \quad (3)$$

$$\rightarrow c\text{-}CH_2(N)CH + H \qquad \Delta H^\circ = -60.2 \text{ kcal mol}^{-1} \quad (4)$$

$$\rightarrow CH_2NCH + H \qquad \Delta H^\circ = -51.4 \text{ kcal mol}^{-1} \quad (5)$$

$$\rightarrow c\text{-}CH(NH)CH + H \qquad \Delta H^\circ = -27.0 \text{ kcal mol}^{-1} \quad (6)$$

where, ΔH° denotes a reaction enthalpy computed at 0 K. The numbering of reaction paths (or product channels) is based on the order of reaction enthalpy. Available energy E_{ava} of a reaction can be calculated based on $E_{ava} = E_c - \Delta H^\circ$. The RRKM and VTST calculations predicted that reactions (1)–(6) have branching ratios ~0, 0.042, 0.023, 0.869, 0.044, and ~0, respectively. Although reaction (1) produces the most stable isomer CH_3CN (acetonitrile), the multiple isomerization processes as shown in Fig. 9 results in almost no yield to this

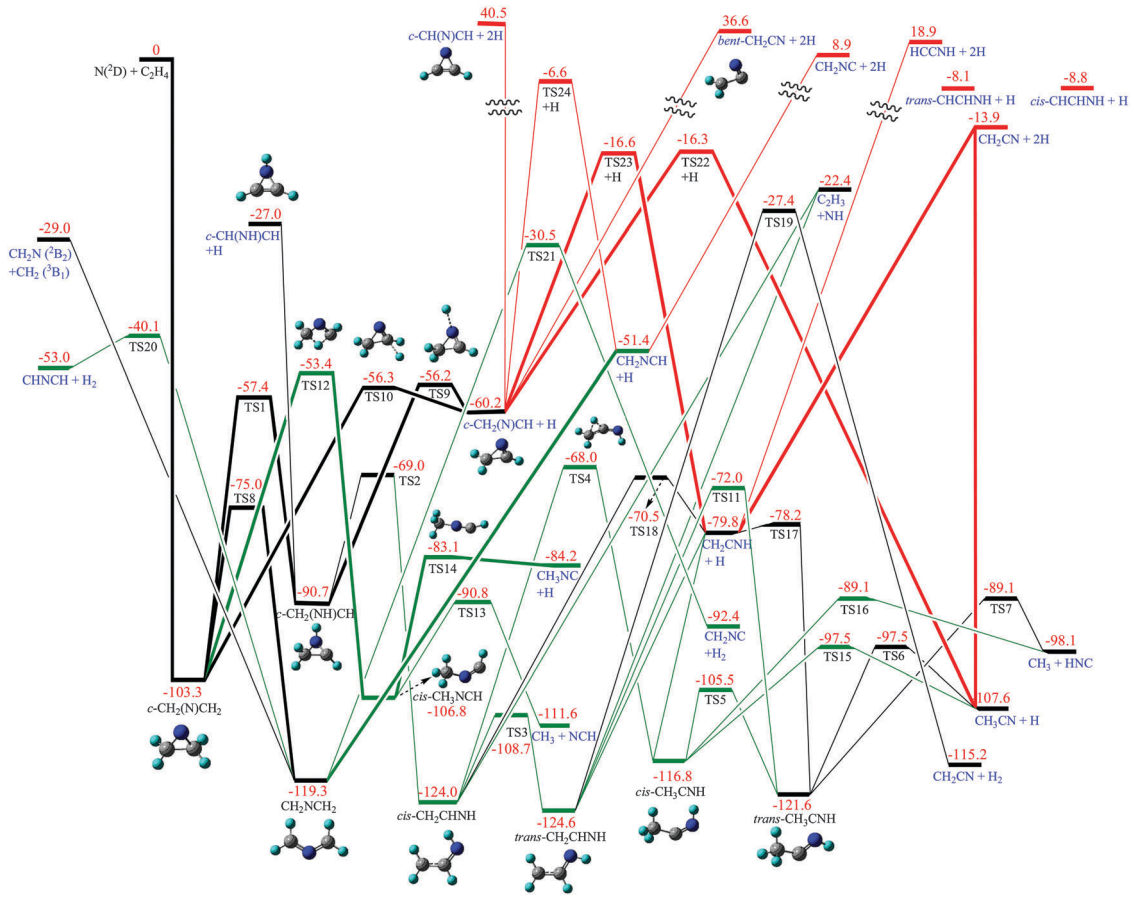

Fig. 9 Potential-energy surface for the reaction $N(^2D) + C_2H_4$. The green and red paths are not calculated in the work of Takayanagi *et al.* Thick solid lines denote some likely pathways leading to products $C_2H_3N + H$ and $C_2H_2N + 2H$.

Table 1 Available energy E_{ava},[a] average kinetic-energy release $\langle E_t \rangle$, and fractions of translational energy f_t for two product channels of reaction $N(^2D) + C_2H_4$ at E_c = 4.3 kcal mol^{-1}

Product channels	$C_2H_3N + H$	$C_2H_2N + 2H$
E_{ava}/kcal mol^{-1}	64.5	18.2
$\langle E_t \rangle$/kcal mol^{-1}	23.1	7.3[b]
f_t (%)	35.8	40.1

[a] The E_{ava} values of the most-probable isomeric channels *c*-$CH_2(N)CH + H$ and $CH_2CN + 2H$ were adopted for the calculations of $\langle E_t \rangle$ and f_t. [b] The $\langle E_t \rangle$ value of the channel $C_2H_2N + 2H$ was derived based on an assumption of a two-body dissociation process with a product mass ratio of 40 : 2.

Table 2 Adiabatic ionization energies (IE) of various isomers of C_2H_3N and C_2H_2N

Species	Theoretical IE[a]/eV	Experimental IE[b]/eV
CH_3CN	12.5	12.20 ± 0.01
CH_3NC	11.2	11.53 ± 0.04
c-$CH_2(N)CH$	9.94	10.1
c-$CH(NH)CH$	8.12	N/A
CH_2CNH	8.64	N/A
CH_2NCH	7.84	N/A
CH_2CN	10.2	9.9 ± 0.1
CH_2NC	9.28	N/A
CHNCH	8.66	N/A

[a] The present values calculated at the level of CCSD(T)/6-311+G(3df,2p)//B3LYP/6-311G(d,p) + ZPE[B3LYP/6-311G(d,P)]. [b] Quoted from NIST Chemistry WebBook: http://webbook.nist.gov/chemistry/.

product. Fig. 9 indicates that reaction complex *c*-$CH_2(N)CH_2$ might directly eject a hydrogen atom through TS10 to produce *c*-$CH_2(N)CH$ (2*H*-azirine) (reaction 4a). In addition, one of hydrogen atoms of *c*-$CH_2(N)CH_2$ might migrate to the nitrogen atom to form *c*-$CH_2(NH)CH$ that subsequently ejects the hydrogen atom through TS9 to produce *c*-$CH_2(N)CH$ (reaction 4b). Reactions (4a) and (4b) were predicted to have branching ratios 0.819 and 0.05, respectively, by RRKM calculations. *c*-$CH_2(NH)CH$ can rupture the CH_2–NH bond to form *cis*-CH_2CHNH that subsequently decomposes to CH_2CNH (ketene imine) + H through TS18 (reaction 3). Because of large dissociation energy, the decomposition from *c*-$CH_2(NH)CH$ to *c*-$CH(NH)CH + H$ (reaction 6) was predicted to be negligible by RRKM calculations. *c*-$CH_2(N)CH_2$ can break the C–C bond through TS8 to form planar intermediate CH_2NCH_2 that subsequently breaks one of bonds C–H to produce $CH_2NCH + H$ (reaction 5). *c*-$CH_2(N)CH_2$ can rearrange also to *cis*-CH_3NCH through TS12 followed by decomposition to CH_3NC (methyl isocyanide) + H (reaction 2). Takayanagi *et al.* ignored reactions (2) and (5) that were predicted to have non-negligible branching ratios by RRKM calculations.

Table 3 Calculated product branching ratios for the decomposition of complex *c*-$CH_2(N)CH_2$ from the $N(^2D) + C_2H_4$ reaction

Labels	Products	Branching ratios[a] (%)	Branching ratios[b] (%)
1	$CH_3CN + H$	0.03	0.8
2	$CH_3NC + H$	4.18	N/C
3	$CH_2CNH + H$	2.28	13.2
4	*c*-$CH_2(N)CH + H$	86.91 (= 81.93[c] + 4.98[d])	84.8
5	$CH_2NCH + H$	4.40	N/C
6	*c*-$CH(NH)CH + H$	~0	~0
12	$CH_2CN + H_2$	~0	~0
13	$CH_2NC + H_2$	0.21	N/C
14	$CHNCH + H_2$	1.17	N/C
15	$CH_3 + NCH$	0.39	N/C
16	$CH_3 + HNC$	0.09	1.2
17	$CH_2N + CH_2$	0.34	~0
18	$C_2H_3 + NH$	~0	~0

[a] Calculated at E_c = 5 kcal mol^{-1} in the present work. [b] Calculated at E_c = 0 kcal mol^{-1} by Takayanagi *et al.* (ref. 14); N/C denotes "Not Considered". [c] For reaction (4a). [d] For reaction (4b).

The maximal kinetic-energy release is in good agreement with the energetic limit of reaction (4) and the ionization threshold of C_2H_3N is in good agreement with the IE of CH_2NCH from reaction (5). Thus, isomers *c*-$CH_2(N)CH$ and CH_2NCH might have contributions to product C_2H_3N although the TOF distributions of product C_2H_3N shown as the red curves in Fig. 3 have no significant change with the increase of photon energy from 9.6 eV to 11.7 eV. Since atomic hydrogen fragment carries no internal energy, the distribution of internal energy (E_{int}) of product C_2H_3N can be derived directly based on $P(E_{int}) = P(E_{ava} - E_t)$. *c*-$CH_2(N)CH$, if produced alone, will have average internal energy 41.4 kcal mol^{-1} (1.80 eV), which might cause a red shift in the ionization threshold to some extent. *c*-$CH_2(N)CH_2$ was calculated to have moments of inertia I_A = 19.130 uÅ^2, I_B = 23.107 uÅ^2, and I_C = 35.506 uÅ^2. The present RRKM calculations indicate that reaction complex *c*-$CH_2(N)CH_2$ has a decay rate ~4.52×10^{12} s^{-1} corresponding to a lifetime of 0.22 ps that is shorter than rotational periods 13.4, 16.2 and 24.8 ps of *c*-$CH_2(N)CH_2$ with L = 1 along principal axes *a*, *b* and *c*, respectively. In the theoretical study of reaction $N(^2D) + H_2 \rightarrow NH + H$, the angular distribution of NH was nearly forward–backward symmetric with a slight bias towards backward scattering at low collision energy.[4] Deviations from symmetry arose when small impact parameters (small L values) were favored, as then reactions favored backward scattering in hydrogen-atom elimination.[4] This argument is applicable also to the present result of backward-biased angular distribution. TS10 in the dominant reaction path (4a) has the leaving hydrogen atom to be recoiled preferentially into the backward hemisphere. Rotational periods become 0.40, 0.48 and 0.74 ps for L = 47 along principal axes *a*, *b* and *c*, respectively; this L value is calculated with b = 1.636 Å estimated from the equilibrium structure of *c*-$CH_2(N)CH_2$. Thus, products could be scattered into the forward and backward hemispheres for large L values. The angular distribution behaves forward-backward (or sideways) peaking when products are recoiled preferentially perpendicular (or parallel) to $\vec{L}$ based on a statistical model.[31] The angular distribution behaves nearly isotropic when products are recoiled into a wide angular range with respect to vector $\vec{L}$.[31]

B Reaction $N(^2D) + C_2H_4 \rightarrow C_2H_2N + 2H$

The contribution from internally-excited C_2H_3N (*e.g.*, *c*-$CH_2(N)CH$) to $C_2H_2N^+$ by dissociative photoionization is negligible herein based on the following reasons. First, the enthalpy of reaction *c*-$CH_2(N)CH \rightarrow CH_2CN^+ + H + e^-$ was calculated to be 12.2 eV; thus, product *c*-$CH_2(N)CH$ requires internal energy at least 50.7 kcal mol^{-1} (2.2 eV), which is larger than the barrier height 43.6–43.9 kcal mol^{-1} of isomerization and the enthalpy 46.3 kcal mol^{-1} of dissociation *c*-$CH_2(N)CH \rightarrow CH_2CN + H$, to undergo this dissociative ionization process with photon energy 10 eV. Second, Fig. 1 indicates that the species with m/z = 40 u has a TOF distribution insensitive to the photoionization energy from 15.1 to 10.8 eV (even down to 10.2 eV but not shown therein) and quite different from that of the species with m/z = 41 u. Third, the bimodal feature of m/z = 41 u in TOF distributions at scattering angles near Θ_{cm} remains as the photoionization energy is below the appearance threshold 10 eV of species with m/z = 40 u; Fig. 3 presents the TOF spectra of m/z = 41 u recorded at 9.6 eV. Fourth, Fig. 8 indicates that the appearance threshold of $C_2H_2N^+$ is in good agreement with the ionization energy of CH_2CN. Accordingly, the signal observed at m/z = 40 u is attributed mainly to product C_2H_2N rather than a daughter ion of product C_2H_3N.

To account for the production of $C_2H_2N + 2H$, we calculated the following five isomeric channels as shown in Fig. 9.

$$N(^2D) + C_2H_4 \rightarrow CH_2CN + 2H \qquad \Delta H^\circ = -13.9 \text{ kcal mol}^{-1} \quad (7)$$

$$\rightarrow CH_2NC + 2H \qquad \Delta H^\circ = 8.9 \text{ kcal mol}^{-1} \quad (8)$$

$$\rightarrow HCCNH + 2H \qquad \Delta H^\circ = 18.9 \text{ kcal mol}^{-1} \quad (9)$$

$$\rightarrow \textit{bent}\text{-}CH_2CN + 2H \qquad \Delta H^\circ = 36.6 \text{ kcal mol}^{-1} \quad (10)$$

$$\rightarrow c\text{-}CH(N)CH + 2H \qquad \Delta H^\circ = 40.5 \text{ kcal mol}^{-1} \quad (11)$$

bent-CH_2CN and *cyclic*-CH(N)CH (*c*-CH(N)CH) can be produced from successive elimination of two hydrogen atoms from the same and from different carbon atoms, respectively, of reaction complex *c*-$CH_2(N)CH_2$. Only reaction (7) is energetically accessible in the present work. C_2H_2N can also be produced by elimination of a hydrogen molecule as the following three reactions.

$$N(^2D) + C_2H_4 \rightarrow CH_2CN + H_2 \qquad \Delta H^\circ = -115.2 \text{ kcal mol}^{-1} \quad (12)$$

$$\rightarrow CH_2NC + H_2 \qquad \Delta H^\circ = -92.4 \text{ kcal mol}^{-1} \quad (13)$$

$$\rightarrow CHNCH + H_2 \qquad \Delta H^\circ = -53.0 \text{ kcal mol}^{-1} \quad (14)$$

The production of C_2H_2N by elimination of a hydrogen molecule cannot satisfactorily account for the experimental observations based on the following reasons. First, a reaction like (12)–(14) having a large exothermicity and a large exit barrier typically recoils products into large translational energy; however, Fig. 7 indicates that the maximal kinetic-energy

release is near the energetic limit of reaction (7). Second, if products from reactions (12)–(14) have small kinetic energy release like that in Fig. 7, C_2H_2N will be predicted to have a large internal energy and have a considerable red shift in the ionization threshold; however, Fig. 8 indicates that the ionization threshold of C_2H_2N is in good agreement with the ionization energy of CH_2CN (cyanomethyl). Product CH_2CN from reaction (7) has an average internal energy merely 10.9 kcal mol^{-1} (0.47 eV). Third, reactions (12)–(14) have negligible branching ratios based on RRKM calculations. Thus, reaction (7) is the most likely channel for the production of C_2H_2N.

Fig. 9 presents four pathways for the production of $CH_2CN + 2H$ from the spontaneous dissociation of products CH_3CN, CH_2CNH, and *c*-$CH_2(N)CH$.

$$CH_3CN \rightarrow CH_2CN + H \qquad \Delta H^\circ = 93.7 \text{ kcal mol}^{-1} \quad (1')$$

$$CH_2CNH \rightarrow CH_2CN + H \qquad \Delta H^\circ = 65.9 \text{ kcal mol}^{-1} \quad (3')$$

$$c\text{-}CH_2(N)CH \rightarrow CH_3CN \rightarrow CH_2CN + H \qquad \Delta H^\circ = 46.3 \text{ kcal mol}^{-1} \quad (4')$$

$$c\text{-}CH_2(N)CH \rightarrow CH_2CNH \rightarrow CH_2CN + H \qquad \Delta H^\circ = 46.3 \text{ kcal mol}^{-1} \quad (4'')$$

CH_3CN and CH_2CNH can decompose to $CH_2CN + H$ without barriers. In contrast, *c*-$CH_2(N)CH$ needs isomerization to CH_3CN and CH_2CNH through TS22 and TS23, respectively, before decomposition to $CH_2CN + H$. TS22 lies 2.4 kcal mol^{-1} and TS23 2.7 kcal mol^{-1} below asymptote $CH_2CN + H$, which makes reactions (4′) and (4″), possible. We suggest that reactions (4′) and (4″) are more important than reactions (1′) and (3′) since reaction (4) is much more dominant than reactions (1) and (3) by RRKM calculations. This suggestion coincides with the experimental finding that the channel $C_2H_2N + 2H$ is about 5.7 times the branching ratio of the channel $C_2H_3N + H$. CH_2NCH can rearrange to *c*-$CH_2(N)CH$ through TS24 and subsequently undergoes reactions (4′) and (4″); this reaction path has a possible contribution only to the products with E_t less than 10.9 kcal mol^{-1} because of the large isomerization barrier (TS24) lying 7.3 kcal mol^{-1} above asymptote $CH_2CN + H$.

C. Branching ratios

Branching ratios for channel $C_2H_3N + H$ to channel $C_2H_2N + 2H$ was estimated to be 15 : 85 from the c.m. ion signals of products C_2H_3N and C_2H_2N recorded with photoionizing energy 11.7 eV on assuming both products have the same detection efficiency. The contribution of isotopomers of C_2H_2N to the signal of $m/z = 41$ u was removed. It might not be quantitatively accurate enough in the present analysis without a calibration of detection efficiency (*e.g.* ionization cross sections) but the channel $C_2H_2N + 2H$ should be doubtless greater than the channel $C_2H_3N + H$ in branching. RRKM calculations predict that reaction (4) is overwhelmingly dominant among two-body dissociation channels. Thus, most of nascent C_2H_3N products, notably *c*-$CH_2(N)CH$, are suggested to further decompose to $CH_2CN + H$ in order to rationalize the experimental branching ratios. Other energetically accessible product channels unobserved in experiments are listed below.

$$N(^2D) + C_2H_4 \rightarrow CH_3 + HCN \qquad \Delta H^\circ = -111.6 \text{ kcal mol}^{-1} \quad (15)$$

$$\rightarrow CH_3 + HNC \qquad \Delta H^\circ = -98.1 \text{ kcal mol}^{-1} \quad (16)$$

$$\rightarrow CH_2N + CH_2 \qquad \Delta H^\circ = -29.0 \text{ kcal mol}^{-1} \quad (17)$$

$$\rightarrow C_2H_3 + NH \qquad \Delta H^\circ = -22.4 \text{ kcal mol}^{-1} \quad (18)$$

Although reactions (15) and (16) have large exothermicities, Fig. 9 indicates that the multi-isomerization processes with large barriers diminish the dissociation probability. Reactions (17) and (18) have small exothermicities and thus lose competition based on RRKM calculations.

D Comparison with previous works

In the experimental part, we explicitly observed two products C_2H_3N and C_2H_2N using selective photoionization. In contrast, Balucani *et al.* claimed that they observed product C_2H_3N at $m/z = 40$ u using electron-impact ionization.[16] Fig. 1 and 3 indicate that the contribution of isotopic variants of C_2H_2N to $m/z = 41$ u increases and the TOF distribution of $m/z = 41$ u becomes similar to that of $m/z = 40$ u with the increase of photoionization energy, which accounts for the reason why Balucani *et al.* misrecognized the species of $m/z = 40$ u as daughter ions of the species with $m/z = 41$ u. In another words, what they reported are the results of product C_2H_2N rather than C_2H_3N. On the other hand, the forward-biased angular distribution reported by Balucani *et al.*[16] at $E_c = 8$ kcal mol^{-1} differs from the present result having a slight bias to the backward part at $E_c = 4.3$ kcal mol^{-1}. The collision-energy dependence of product angular distributions was observed also in the reaction of $N(^2D) + C_2H_2 \rightarrow HCCN + H$;[13] the angular distribution of HCCN was isotropic at $E_c = 3.1$ kcal mol^{-1} and became forward preferred at $E_c = 9.5$ kcal mol^{-1}. Balucani *et al.*[13] indicated that at low collision energy the lifetime of a persistent reaction complex (or intermediate) is longer than its rotational period but at high collision energy the lifetime of an osculating complex is comparable to its rotational period and an osculating model[30,32] is applicable. Accordingly, the collision-energy effect can account for the difference between the present work and Balucani's *et al.* in product angular distributions.

In the computational part, we established a more complete potential-energy surface than the work of Takayanagi *et al.*[14] for the $N(^2D) + C_2H_4$ reaction. Takayanagi *et al.* ignored the *cis–trans* isomerization processes of intermediates CH_2CHNH and CH_3CNH, the dissociation pathways leading to $CH_3NC + H$ (reaction 2), $CH_2NCH + H$ (reaction 5), $CH_2NC + H_2$ (reaction 13), $CHNCH + H_2$ (reaction 14) and $CH_3 + NCH$ (reaction 15), and the secondary dissociation pathways leading to various isomers of $C_2H_2N + 2H$. The complements (color lines in Fig. 9) make a satisfactory explanation possible for the experimental observations as addressed in the above sections. For instance, the ionization threshold of product C_2H_3N is in good agreement with the IE of CH_2NCH, indicating that reaction (5), in addition to

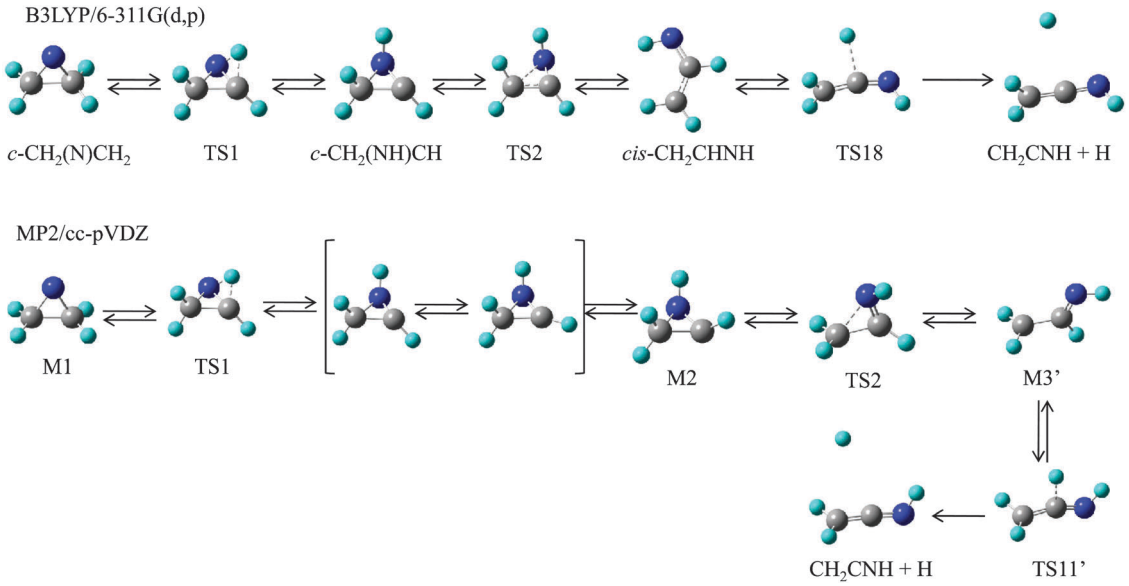

Fig. 10 The stationary and transition structures of reaction complexes and intermediates situating on the reaction path (3) computed by two methods of B3LYP/6-311G(d,p) (upper) and MP2/cc-pVDZ (lower). The present notations are employed in the upper path but the notations of Takayanagi *et al.* (ref. 14) are employed in the lower path. Two structures in a bracket are ignored in the work of Takayanagi *et al.* M3′ (TS11′) differs from M3 (TS11) computed by Takayanagi *et al.*

reaction (4), might have a contribution to product C_2H_3N. Furthermore, channel C_2H_2N+2H is about 5.7 times the branching of channel C_2H_3N+H, indicating that most of primary product *c*-$CH_2(N)CH$ from reaction (4) further decomposes to CH_2CN+H, consistent with quantum-chemical calculations. In the part (black lines in Fig. 9) similar to the work of Takayanagi *et al.*,[14] the energies of intermediates and products relative to reactant $N(^2D)+C_2H_4$ differ from the present computational values within ± 3 kcal mol^{-1} except for intermediate CH_2CHNH (*vide infra*). Some of the molecular structures computed in the present work differ from those reported by Takayanagi *et al.* mainly on molecular conformations. Fig. 10 presents the optimized structures of molecules situating on reaction path (3) leading to product CH_2CNH+H computed with two methods of B3LYP/6-311G(d,p) (upper path) and MP2/cc-pVDZ (lower path). The molecular structures of B3LYP/6-311G(d,p) correspond to the stationary and transition states of reaction path (3) shown in Fig. 9. The connection of a transition structure with its reactant and product was verified with the calculation of IRC. On the other hand, the lower path of Fig. 10 shows the results of method MP2/cc-pVDZ same as those of Takayanagi *et al.* but with some corrections; the same notations as those of Takayanagi *et al.* were adopted in the lower path. For instance, *c*-$CH_2(NH)CH$ presented in the upper path of Fig. 10 has a conformation with dihedral angle $\angle HCNH = -127.7^\circ$ but Takayanagi *et al.* reported another conformer M2 that has $\angle HCNH = -15.0^\circ$. M2 cannot correlate directly with TS1 without the two additional structures shown in a bracket. M3′ and TS11′ differ from M3 and TS11 reported by Takayanagi *et al.* M3′ (TS11′) has a reflection operator bisecting the methyl group and has a point group C_s but M3 (TS11) has a point group C_1. Moreover, M3 is likely an electronic excited state lying $\sim$17 kcal mol^{-1} above *cis*-CH_2CHNH.

VI. Conclusions

This work explored the dynamics of reaction of atomic N in state ^2D with ethene (C_2H_4) at collision energy E_c = 4.3 kcal mol^{-1} by interrogating product channels C_2H_3N+H and C_2H_2N+2H. We measured kinetic-energy distributions, angular distributions, and photoionization spectra of products C_2H_3N and C_2H_2N. Furthermore, we established a comprehensive doublet PES for the $N(^2D)+C_2H_4$ reaction and calculated branching ratios of various product channels at E_c = 5 kcal mol^{-1} using RRKM and VTST approaches. The combination of experimental and theoretical results unveils the reaction mechanisms. The $N(^2D)$ atom adds to the C=C π-bond of ethene to form a cyclic complex *c*-$CH_2(N)CH_2$ that subsequently undergoes various dissociation pathways. *c*-$CH_2(N)CH_2$ mainly ejects one of the hydrogen atoms to produce *c*-$CH_2(N)CH+H$ with a branching ratio 0.87 predicted by RRKM calculations. Most of *c*-$CH_2(N)CH$ further decompose to CH_2CN+H following isomerization to CH_3CN or CH_2CNH, which rationalizes the experimental branching ratios of 15 : 85 for channel C_2H_3N+H to channel C_2H_2N+2H. The angular distribution of C_2H_3N has a propensity to the backward part, implying that *c*-$CH_2(N)CH_2$ is a short-lived complex compared with its rotational period. Measurements of kinetic-energy release and ionization thresholds allowed us to identify product C_2H_3N as a mixture of *c*-$CH_2(N)CH$ and CH_2NCH as well as product C_2H_2N as CH_2CN. The present work corrects the previous work of Balucani *et al.*, elucidating the merits of selective photoionization with synchrotron radiation as an ionization source.

Acknowledgements

We thank National Synchrotron Radiation Research Center, Academia Sinica, and the National Science Council of Taiwan (Grants NSC97-2113-M-213-003-MY3 and NSC99-2811-M-213-003) for supports.

References

1 W. L. Wiese, M. W. Smith, and B. M. Glennon, *Atomic Transition Probabilities*, Natl. Bur. Stand. Ref. Data Ser., Natl. Bur. Stand. (U.S.), Circ. No. 4 (U.S. GPO, Washington, D. C., 1966).
2 Chemical kinetics data from NIST web page: http://kinetics.nist.gov/kinetics/index.jsp.
3 H. Umemtot, T. Asai and Y. Kimura, *J. Chem. Phys*., 1997, **106**, 4985.
4 L. A. Pederson, G. C. Schatz, T.-S. Ho, T. Hollebeek, H. Rabitz, L. B. Harding and G. Lendvay, *J. Chem. Phys*., 1999, **110**, 9091.
5 N. Balucani, M. Alagia, L. Cartechini, P. Casavecchia, G. G. Volpi, L. A. Pederson and G. C. Schatz, *J. Phys. Chem. A*, 2001, **105**, 2414.
6 H. Umemoto, T. Asai, H. Hashimoto and T. Nakae, *J. Phys. Chem. A*, 1999, **103**, 700.
7 H. Umemoto, Y. Kimura and T. Asai, *Chem. Phys. Lett*., 1997, **264**, 215.
8 H. Umemoto, T. Nakae, H. Hashimoto, K. Kongo and M. Kawasaki, *J. Chem. Phys*., 1998, **109**, 5844.
9 Y. Kurosaki, T. Takayanagi, K. Sato and S. Tsunashima, *J. Phys. Chem. A*, 1998, **102**, 254.
10 W.-K. Chen, I.-C. Lu, C. Chaudhuri, W.-J. Huang and S.-H. Lee, *J. Phys. Chem. A*, 2008, **112**, 8479.
11 I.-C. Lu, W.-K. Chen, C. Chaudhuri, W.-J. Huang, J. J. Lin and S.-H. Lee, *J. Chem. Phys*., 2008, **129**, 174304.
12 T. Takayanagi, Y. Kurosaki, K. Misawa, M. Sugiura, Y. Kobayashi, K. Sato and S. Tsunashima, *J. Phys. Chem. A*, 1998, **102**, 6251.
13 N. Balucani, M. Alagia, L. Cartechini, P. Casavecchia, G. G. Volpi, K. Sato, T. Takayanagi and Y. Kurosaki, *J. Am. Chem. Soc*., 2000, **122**, 4443.
14 T. Takayanagi, Y. Kurosaki, K. Sato and S. Tsunashima, *J. Phys. Chem. A*, 1998, **102**, 10391.
15 K. Sato, K. Misawa, Y. Kobayashi, M. Matsui, S. Tsunashima, Y. Kurosaki and T. Takayanagi, *J. Phys. Chem. A*, 1999, **103**, 8650.
16 N. Balucani, L. Cartechini, M. Alagia, P. Casavecchia and G. G. Volpi, *J. Phys. Chem. A*, 2000, **104**, 5655.
17 S.-H. Lee, J. J. Lin and Y. T. Lee, *J. Electron Spectrosc. Relat. Phenom*., 2005, **144–147**, 135.
18 S.-H. Lee, *J. Chem. Phys*., 2009, **131**, 174312.
19 S.-H. Lee, *Phys. Chem. Chem. Phys*., 2010, **12**, 2655.
20 I.-C. Lu, W.-K. Chen, W.-J. Huang and S.-H. Lee, *J. Chem. Phys*., 2008, **129**, 164304.
21 S.-H. Lee, W.-K. Chen and W.-J. Huang, *J. Chem. Phys*., 2009, **130**, 054301.
22 I.-C. Lu, W.-J. Huang, C. Chaudhuri, W.-K. Chen and S.-H. Lee, *Rev. Sci. Instrum*., 2007, **78**, 083103.
23 C.-H. Chin and S.-H. Lee, *J. Chem. Phys*., 2011, **134**, 044309.
24 P. J. Robinson and K. A. Holbrook, *Unimolecular Reactions*, Wiley, New York, 1972.
25 H. Eyring, S. H. Lin and S. M. Lin, *Basic Chemical Kinetics*, Wiley, New York, 1980.
26 J. I. Steinfield, J. S. Francisco and W. L. Hase, *Chemical Kinetics and Dynamics*, Prentice-Hall, Engelwood Cliffs, NJ, 1999.
27 A. M. Mebel, V. V. Kislov and R. I. Kaiser, *J. Phys. Chem*., 2006, **110**, 2421.
28 D. R. Lide, *Handbook of Chemistry and Physics*, CRC, Boca Raton, FL, 78th edn, 1997.
29 From NIST Chemistry WebBook: http://webbook.nist.gov/chemistry/.
30 R. D. Levine and R. B. Bernstein, *Molecular Reaction Dynamics and Chemical Reactivity*, Oxford University Press, New York, 1987.
31 R. Grice, *Int. Rev. Phys. Chem*., 1995, **14**, 315, and references therein.
32 W. B. Miller, S. A. Safron and D. R. Herschbach, *Discuss. Faraday Soc*., 1967, **44**, 108.